Open Ceramics 18 (2024) 100586

Contents lists available at ScienceDirect

Open Ceramics

journal homepage: www.sciencedirect.com/journal/open-ceramics

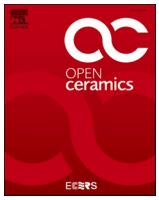

# Processing and cytocompatibility of Cu-doped and undoped *fluoride*-containing bioactive glasses

Q. Nawaz [b,*], C. Blaeß [a], R. Müller [a], A.R. Boccaccini [b]

[a] Bundesanstalt für Materialforschung und -prüfung (BAM), Richard-Willstätter-Straße 11, 12489, Berlin, Germany
[b] Friedrich-Alexander University Erlangen-Nuremberg, Institute of Biomaterials, 910504, Erlangen, Germany

ARTICLE INFO

Handling Editor: Dr P Colombo

*Keywords:*
Bioactive glass
Crystallization
Solubility
Cytocompatibility
Surface roughness

ABSTRACT

Sintered or additive-manufactured bioactive glass (BG) scaffolds are highly interesting for bone replacement applications. However, crystallization often limits the high-temperature processability of bioactive glasses (BGs). Thus, the BG composition must combine high bioactivity and processability. In this study, three BGs with nominal molar (%) compositions 54.6$SiO_2$-1.7$P_2O_3$-22.1CaO-6.0$Na_2O$-7.9$K_2O$-7.7MgO (13–93), 44.8$SiO_2$-2.5$P_2O_3$-36.5CaO-6.6$Na_2O$-6.6$K_2O$-3.0$CaF_2$ (F3) and 44.8$SiO_2$-2.5$P_2O_3$-35.5CaO-6.6$Na_2O$-6.6$K_2O$-3.0$CaF_2$-1.0CuO (F3–Cu) were investigated. The dissolution and ion release kinetics were investigated on milled glass powder and crystallized particles (500–600 μm). All glasses showed the precipitation of hydroxyapatite (HAp) crystals after 7 days of immersion in simulated body fluid. No significant differences in ion release from glass and crystalline samples were detected. The influence of surface roughness on cytocompatibility and growth of pre-osteoblast cells (MC3T3-E1) was investigated on sintered and polished BG pellets. Results showed that sintered BG pellets were cytocompatible, and cells were seen to be well attached and spread on the surface after 5 days of incubation. The results showed an inverse relation of cell viability with the surface roughness of pellets, and cells were seen to attach and spread along the direction of scratches.

## 1. Introduction

Tissue engineering (TE) and regenerative medicine have great potential for repairing and regenerating damaged tissues and organs. Additive manufacturing (AM) has recently appeared as a versatile technology that allows the fabrication of tissue-engineered constructs to mimic the native structure of lost tissues [1]. AM of bone replacement implants made of bioactive glasses (BGs) with controlled crystallization allows the production of complex-shaped bodies with targeted control over implant architecture, degradation, and the potential to release therapeutic ions [2–4].

A challenge related to the AM of BGs is that many BG compositions of high bioactivity can be prone to crystallization when sintered at high temperatures [5,6]. Kinnunen et al. [7] used cast block BG implants in 14 patients for orbital floor fractures. The results indicated that BG implants were well-tolerated and represented a promising repair material for orbital floor fractures. However, in many cases the geometry of the structures that can be fabricated is limited, or post-sintering machining is required to achieve the desired implant shape.

BGs have a high proportion of network modifiers, which lowers the connectivity of the glass network [8]. This results in increased ion mobility, which promotes the tendency to crystallize and limits BG sinterability. For example, 45S5 BG (45$SiO_2$, 24.5CaO, 24.5$Na_2O$, and 6.0$P_2O_5$(wt%)) strongly tends to crystallize, which significantly limits its processability, especially the possibility of sintering 3D porous structures, such crystallization tendency affects also the ability to produce fibers by melt drawing [9–11]. It is well-known that a fully glassy (non-crystalline) structure from 45S5 BG can not be processed from powders [12–14]. Thus, developing a new series of BGs with modified compositions with a low tendency to crystallize is required, which should allow a better processing window. This has been a long-standing goal of the BG research community [15].

Several BG compositions have been put forward over the years, which can be sintered without crystallization, including ICIE16 [16], 13–93 [17], and 13–93 $B^3$ [18] BGs. These glasses can be processed using AM approaches involving sintering [19–23]. Winkel et al. [24] reported the 3D printing of a composite containing 13–93 bioactive glass and hydroxyapatite (HAp) powders. A fully isotropic sintering (750 °C at a rate of 2 K/min) of composites having HAp content of 40 wt%. Was obtained. Qazi et al. [25] compared the effect of 13–93 and 45S5 BGs on

* Corresponding author.
*E-mail address:* qaisar.nawaz@fau.de (Q. Nawaz).

https://doi.org/10.1016/j.oceram.2024.100586
Received 10 October 2023; Received in revised form 4 March 2024; Accepted 22 March 2024
Available online 29 March 2024

**Table 1**
Nominal and actual glass compositions of all glasses measured by XRF.

| Glass | | Chemical composition (mol%) | | | | | | | |
|---|---|---|---|---|---|---|---|---|---|
| | | $SiO_2$ | $P_2O_5$ | MgO | CaO | $Na_2O$ | $K_2O$ | $CaF_2$ | CuO |
| **13–93** | nom. | 54.6 | 1.7 | 7.7 | 22.1 | 6.0 | 7.9 | – | – |
| | XRF | 56.4 ± 1.3 | 0.9 ± 0.1 | 6.8 ± 0.2 | 21.6 ± 0.1 | 6.3 ± 1.4 | 7.8 ± 0.1 | – | – |
| **F3** | nom. | 44.8 | 2.5 | – | 36.5 | 6.6 | 6.6 | 3.0 | – |
| | XRF | 44.3 ± 0.4 | 2.3 ± 0.1 | – | 36.0 ± 1.2 | 7.0 ± 0.2 | 7.0 ± 0.2 | 3.1 ± 0.3 | – |
| **F3–Cu** | nom. | 44.8 | 2.5 | – | 35.5 | 6.6 | 6.6 | 3.0 | 1.0 |
| | XRF | 42.7 ± 0.2 | 2.5 ± 0.1 | – | 37.0 ± 1.2 | 7.3 ± 0.4 | 6.2 ± 0.3 | 2.8 ± 0.6 | 1.4 ± 0.1 |

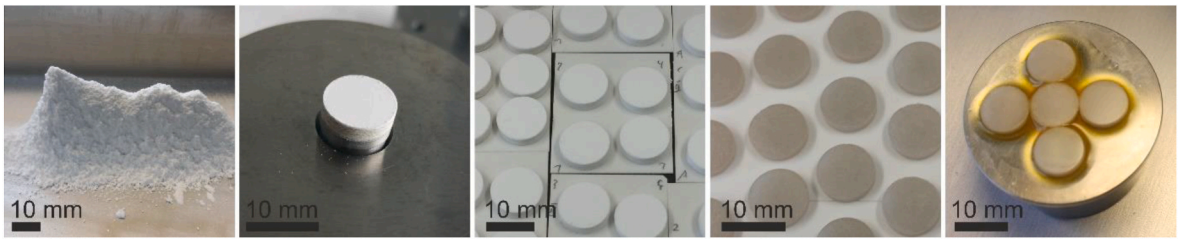


**Fig. 1.** The process of the fabrication of sintered pellets (left to right): glass powder produced by milling and sieving, uniaxial pressing, sintering at 10 K/min of powder compacts to end of shrinkage temperature, and grinding with SiC-grinding discs; Note: This process is shown for 13–93 BG.

**Table 2**
Glass properties measured by DTA, particle size analysis, and Archimedes method.

| Glass | | 13–93 | F3 | F3–Cu |
|---|---|---|---|---|
| | | milled | milled | milled |
| **Particle size fraction (μm)** | $D_{10}$ | 1.4 | 1.3 | 1.5 |
| | $D_{50}$ | 5.2 | 5.5 | 6.9 |
| | $D_{90}$ | 25.5 | 31.6 | 41.2 |
| **Glass transition (°C)** | $T_g$ | 577 | 549 | 546 |
| **Bulk density (g/cm$^3$)** | ρ | 2.64 | 2.77 | 2.78 |

human mesenchymal stromal cells (hMSCs) in three distinct modes: (a) direct contact; and dissolution products in (b) 2D, and (c) 3D culture. It was noticed that 13–93 BG showed good results comparable to 45S5 BG concerning the activity of connective tissue cells. However, ICIE16 and 13–93 glasses have a lower solubility and bioactivity than 45S5 BG [26]. Bioceramics such as HAp or CaP, which have an even lower solubility due to their crystalline structure [27,28], are sometimes not entirely resorbed by the living organism even after years [29].

Therefore, developing bioactive glasses with an optimally adjusted tendency to crystallize about a well-balanced relationship between solubility and sinterability (or crystallization tendency) is necessary to produce implants using AM processes successfully. Groh et al. [26] developed fluoride-containing glasses having solubility comparable to 45S5 BG, but exhibiting a more extensive processing window, allowing the sintering of glassy scaffolds [30] or the drawing into fibers [31]. However, there is still a need to understand the influence of surface roughness, crystallinity, porosity, and pore architecture on bioactivity and cytocompatibility of fluoride-containing BGs.

In this work, we investigated the surface roughness effects on the interaction of BG surfaces with pre-osteoblast MC3T3-E1 cells. We compared the cytocompatibility and processing of three different compositions named 13–93, F3, and F3–Cu (see compositions in Table 1). Because of the expected pronounced crystallization tendency of BGs, the influence of crystallinity on the degradation behavior in SBF was investigated on F3 BG as representative of the other mentioned compositions.

## 2. Materials and methods

### 2.1. Production of bioactive glasses

Three BGs, named 13–93, F3 and F3–Cu, were investigated in the current study. Glasses were prepared using melt-quenching and reagent grade $SiO_2$, $CaCO_3$, $NaPO_3$, $Na_2CO_3$, $K_2CO_3$, $MgCO_3$, CuO, and $CaF_2$ were used. Batches of 4500 g were molten in a 2-L Pt crucible at 1350 °C. The molten mixture was water quenched to obtain glass frits. The molten mixture was casted in steel moulds to obtain bulk samples.

### 2.2. Powder characterization

Glass composition was determined by X-ray fluorescence microscopy (XRF Zetium Ultimate, Malvern Panalytical B·V., Almelo, Netherlands) using a 4-kW Rh radiation source on three cubic bulk samples of around 28 mm height for 20 min. Fluoride content was checked supplementary by fluorosensitive electrode depending on DIN 51084:2008–11.

X-ray diffraction (XRD) analysis was carried out in the 2θ range of 5–80° with steps of 0.02° each using Cu Kα radiation and a Lynxeye detector on a D8 Discover diffractometer (Bruker AXS, Karlsruhe, Germany).

Bulk glass density was determined by Archimedes-method in deionized water using a balance Kern 770 (Kern & Sohn, Germany).

Glass powders were obtained by crushing the frits using zirconia jars (BB51, Retsch, Haan, Germany). Crushed glass frits were sieved to fractions (500–600) μm, (315–500) μm, and <200 μm for 13–93 and F3–Cu and <125 μm for F3. Planetary ball milling was done using 7 g of particle size fraction (315–500) μm in 200 mL zirconia jars using zirconia balls. The dried samples were first milled for 5 min at 800 rpm using 7 zirconia balls (Ø 10 mm) and homogenized at 400 rpm for 1 min using 100 g of zirconia balls of (2–3) mm diameter. Particles in size of (500–600) μm were fully crystallized on corundum substrates (Keralpor 96, Kerafol, Germany) in a muffle furnace (Netzsch B180, Netzsch, Selb, Germany) by heating at 20 K/min to a holding time of 20 min at 840 °C.

Glass powders were stored in gas-tight sealed glass bottles to prevent further uptake of water and $CO_2$ from the atmosphere. Particle size distribution was determined by light scattering (Mastersizer; Malvern, Worcestershire, UK) of 10 mg dispersed glass powder in a 0.003 M $Na_4P_2O_7$ solution.

Glass transition temperature and crystallization behaviour were

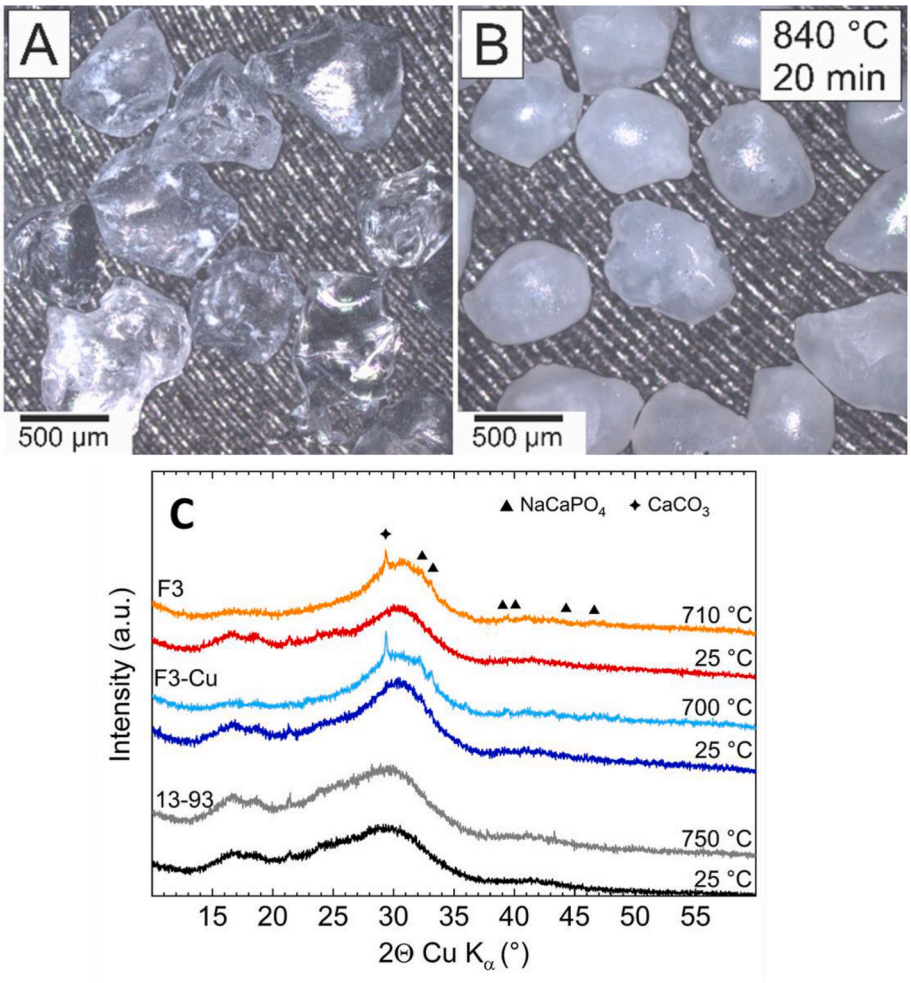


**Fig. 2.** F3 particle size fraction (500–600) µm; (A) before heat treatment and (B) after surface crystallization by heating at 20 K/min to 840 °C for 20 min on corundum substrate. (C) XRD patterns before and after heat-treatment of 13–93, F3 and F3–Cu powders.

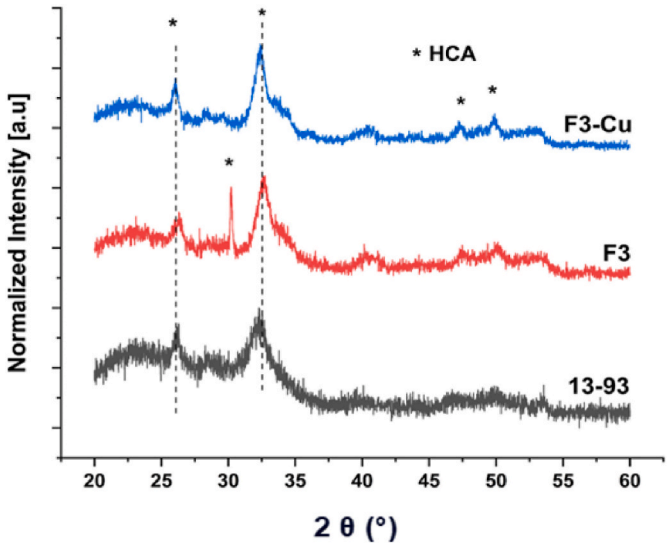


**Fig. 3.** XRD patterns of BG powders after 7 days of immersion in SBF. The XRD patterns indicate the formation of hydroxyapatite ($Ca_{10}(PO_4)_6(OH)_2$ crystalline phase.

monitored in flowing synthetic air (45 mL/min) on (12–16) mg bulk samples placed in open Pt crucibles and heated at 10 K/min using a thermobalance TAG24 (Setaram, Caluire, France).

### 2.3. Fabrication of pellets

Pellets (diameter of 10.5 mm and 5 mm height) were produced by uniaxial pressing the respective powders at 50 MPa for 30 s. Sieved broad particle size fractions <200 µm (13–93 and F3–Cu) and <125 µm (F3) were used to promote higher green body densities and to reach glassy, dense sintered bodies. Pressed powder compacts were heated in a muffle furnace at 10 K/min to their end of shrinkage temperatures and were quenched at 30 K/min cooling rate. The sintering behaviour was determined at 10 K/min using a heating microscope (Erhitzungsmikroskop, Leitz, Wetzlar, Germany) with 7 K accuracy on cylindrical powder compacts of 5 mm in diameter and height. The optimal sintering temperatures were 745 °C, 740 °C, and 690 °C for 13–93, F3, and F3–Cu glasses, respectively. Automated grinding/polishing was done using SiC disks of grades 500, 1200, and 2000 at 150 rpm using 35 N contact pressure for 2 min in counter rotation (Struers, Ballerup Sogn, Denmark). Ethanol (99.7% purity) was used to reduce surface corrosion. The process chain is illustrated schematically in Fig. 1.

Sintered powder compacts and crystallized particles were studied using laser scanning microscopy LSM (Olympus, Tokio, Japan) equipped with white light and (400–420) nm laser light source.

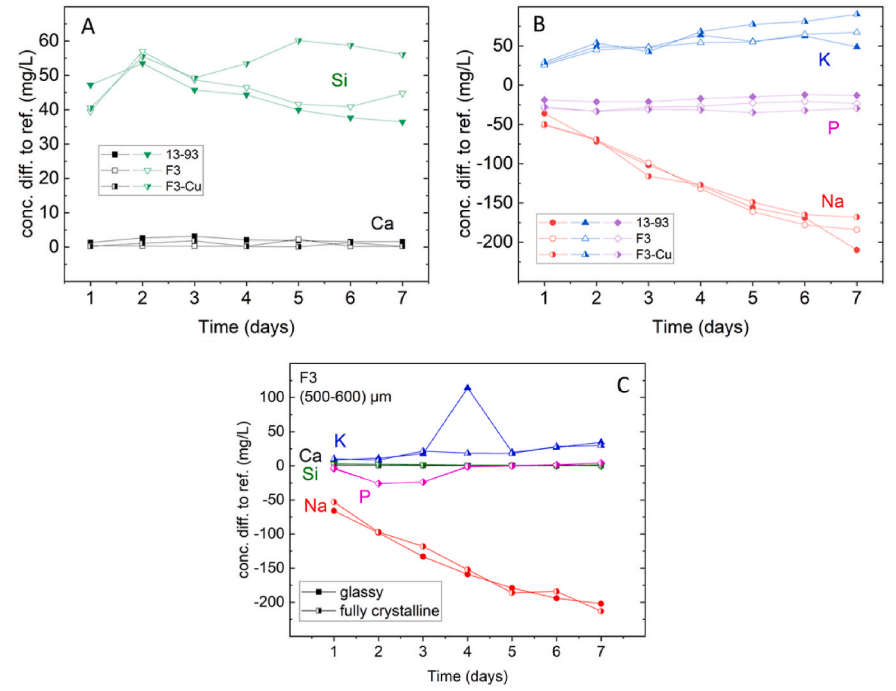


**Fig. 4.** Ion release profile obtained from aliquots of all BG powders after soaking in PBS for 7 days (A and B) and F3 amorphous and crystalline powders (C). The displayed data shows the daily released values and not cumulative concentrations. The increase of potassium on the fourth day should be assigned to a measurement error due to the readjustment after five days. In order to understand more detailed ion release behavior, more extensive investigations are necessary, which exceed the questions investigated here.

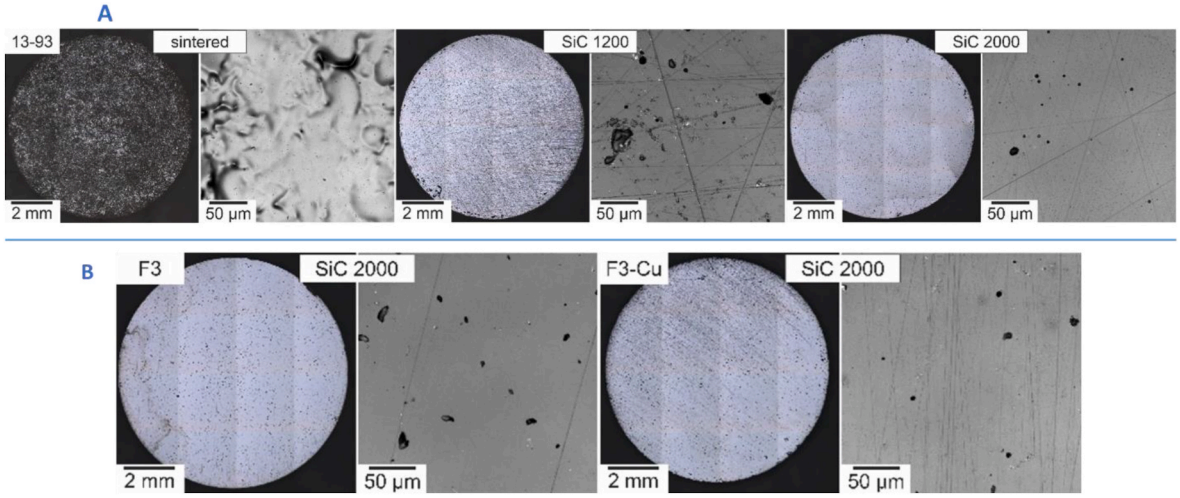


**Fig. 5.** (A) LSM images of 13–93 pellets after sintering to 745 °C at 10 K/min before and after polishing with SiC grinding discs grade 1200 and 2000 and (B) LSM images of F3 and F3–Cu glass pellets heated to 740 °C and 690 °C at 10 K/min and polished with SiC-2000 paper.

**Table 3**
Roughness of sintered and polished pellets as average value with standard deviation, SD, measured via LSM; Sz (µm): roughness depth (peak-to-valley height); Sa(µm): average roughness value.

| | 13–93 | | | | | | F3 | | F3–Cu | |
|---|---|---|---|---|---|---|---|---|---|---|
| | sintered | | SiC 1200 | | SiC 2000 | | SiC 2000 | | SiC 2000 | |
| (µm) | Sz | Sa | Sz | Sa | Sz | Sa | Sz | Sa | Sz | Sa |
| average | 0.124 | 0.035 | 0.130 | 0.022 | 0.044 | 0.007 | 0.034 | 0.005 | 0.053 | 0.008 |
| SD | 0.084 | 0.016 | 0.090 | 0.015 | 0.023 | 0.003 | 0.020 | 0.002 | 0.016 | 0.002 |

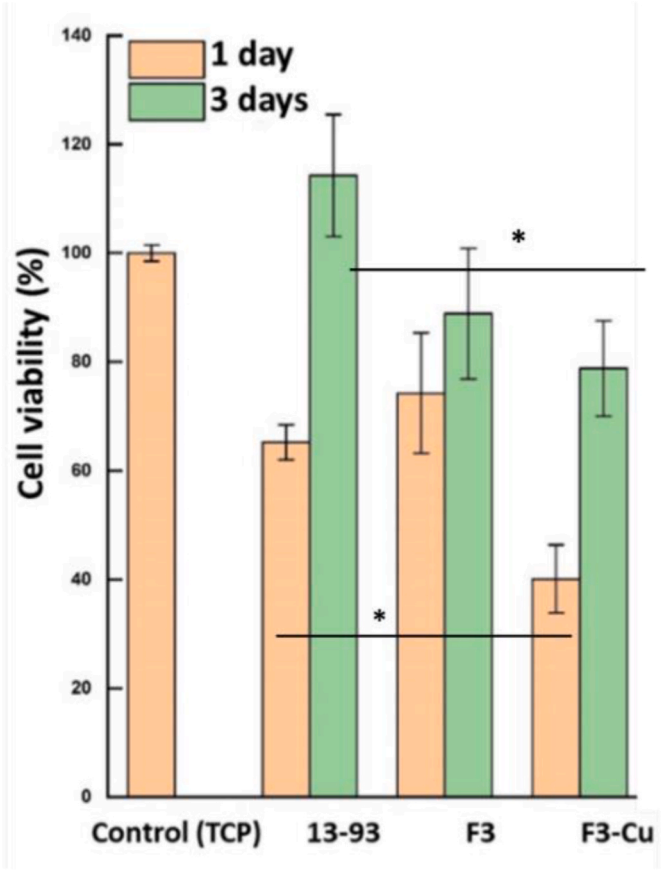


**Fig. 6.** Cell viability of aliquots (1 mL) of BG powders using MC3T3-E1 cells after 1 and 3 days of culture. The tissue culture plate was used as a control. The samples were triplicated, and the mean values were plotted, including the standard deviations. The cell viability (%) values significantly differ at p value of 0.05 within group (1 and 3 days) and with other groups (13–93, F3 and F3–Cu).

### 2.4. Dissolution and cytocompatibility

The *in-vitro* bioactivity of the produced BG powders was assessed by soaking them in simulated body fluid (SBF), according to Kokubo et al. [32]. For this, powders of all glasses were soaked in SBF in falcon tubes and incubated at 37 °C in an orbital shaker (KS 4000, Ika-Werke GmbH, Staufen, Germany) for 7 days. After a predetermined time, SBF was removed, and samples were washed, dried, and analyzed using electron microscopy, SEM (FESEM, LEO 435VP, Carl Zeiss™ AG) and XRD (D8 Advance, Brucker™).

For the ion release study, glassy and crystalline powders (1 mg/mL) were soaked in phosphate buffered solution (PBS) for 7 days under physiological conditions. The aliquots were removed and were chemically analyzed by inductively coupled plasma optical emission spectrometry (ICP-OES) with an iCAP 6000 (Thermo Fisher Scientific, Waltham, Massachusetts, USA) spectrometer.

### 2.5. In-vitro cell studies

The in-vitro *cellular investigations with* MC3T3-E1 cells (pre-osteoblast cell line, Sigma Aldrich) were carried out via direct and indirect methods. For the indirect approach, aliquots of powders were used. 5 x $10^4$ cells were seeded in each well of a 24-well plate and incubated for 24 h. In parallel, all BG powders at a concentration of 1 (w/v %) were soaked in a cell culture medium and incubated for 24 h. The next day, aliquots were collected and seeded cells were washed with PBS. After washing, 1 mL of aliquots from all samples were added to their respective wells. The cells were allowed to grow for 1 and 3 days under physiological conditions in an incubator (5 % $CO_2$, 37 °C).

In the direct approach, cells (5 x $10^4$) were seeded directly on the pellets. The samples were incubated for 5 days to check the influence of direct contact of pellets (roughness and ion release) with cells for a longer time. The cell culture medium was refreshed after 48 h. After 5 days, the morphology of the attached cells was investigated using SEM. Prior to this, cells attached to the surface of the pellets were fixed using fixing solutions. Lastly, the samples were dehydrated with a series of ethanol (30–99 % purity) treatments and dried using a critical point dryer CPD300 (Leica, Germany).

## 3. Results and discussion

### 3.1. Characterization of glass powders

Table 1 summarizes the nominal and measured chemical compositions of the produced glasses. The measured chemical compositions are almost similar (1 mol% difference) to the actual nominal compositions, but slight changes were noticed. In 13–93 BG, the amount of $P_2O_5$ is nearly halved to the nominal composition. A slight increase (0.3–0.7 mol %) in $Na_2O$ content in all BGs is observed, which has slightly decreased the glass transition temperature of BGs.

The physical and thermal properties of glass powders of (315–500) μm size are shown in Table 2. All milled glasses have approximately the same $D_{10}$ values. The $D_{50}$ values of 13–93 and F3 are also similar. The F3–Cu sample showed a higher $D_{50}$ value. However, $D_{90}$ results indicated an increasing particle size distribution from 13 to 93 to F3 to F3–Cu, which might have an effect on the ion dissolution. Glass bulk densities and transition temperature ($T_g$) measured by DTA match the literature values [31]. The difference of $T_g$ of ≈2 % for 13–93 (587 °C) and ≈5 % for F3 (576 °C) [26] can be attributed to the composition differences, as shown in Table 1.

Fig. 2 (A and B) shows F3 particles of size fraction (500–600) μm before and after heat treatment at 840 °C for 20 min. Grains were separated and arranged on a corundum substrate to prevent sintering necks. The untreated particles exhibited sharp edges due to jar crushing, and these edges were smoothed and adopted a round shape after the heat treatment. The heat treatment suggested the occurrence of early-stage crystallization at the grain boundaries in F3 sample (Fig. 2B), which was also confirmed by XRD analysis. XRD of these crystalline

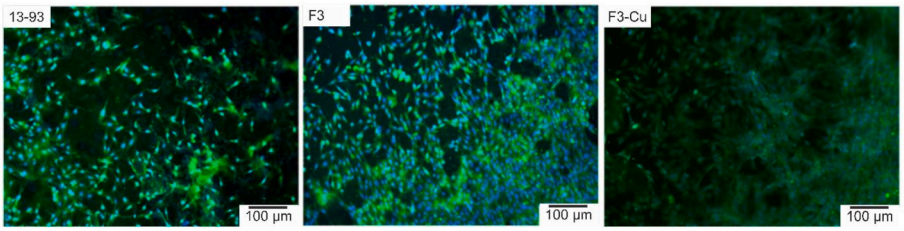


**Fig. 7.** Fluorescence microscopy images of MC3T3-E1 cells showing actin cytoskeleton (blue) and cell nuclei (green) after 3 days of incubation in contact with aliquots (1 mL). (For interpretation of the references to colour in this figure legend, the reader is referred to the Web version of this article.)

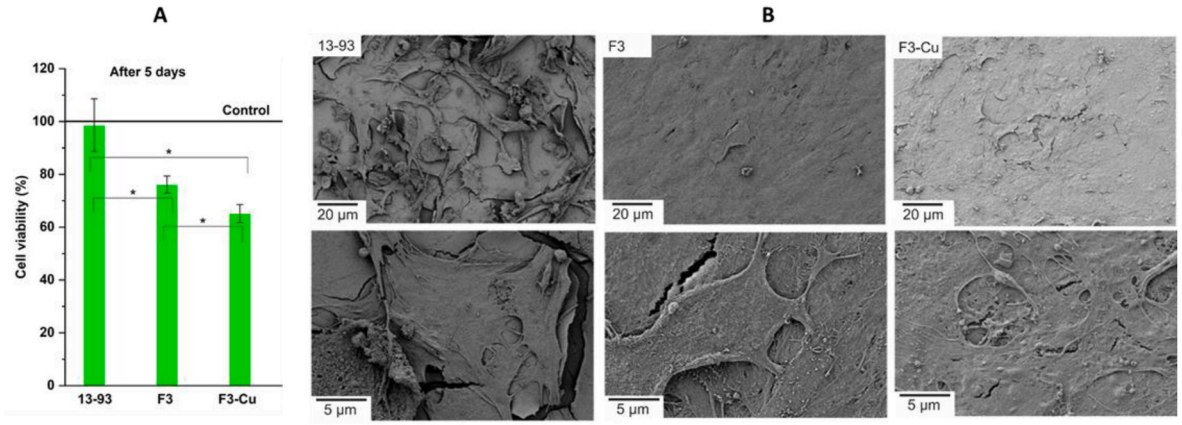


**Fig. 8.** (A) Cell viability of polished pellets using MC3T3-E1 cells after 5 days of culture. The tissue culture plate was used as a control. The samples were triplicated, and mean values and standard deviations were ploted. Viability (%) values significantly differ at p value of 0.05. (B) Morphology at two different magnifications of MC3T3-E1 cells on polished BG pellets (after polishing with SiC 2000 paper) after 5 days of incubation in cell culture medium.

grains detected the traces of $NaCaPO_4$ and $CaCO_3$ as the main crystalline phases, which is also reported in the literature [11,33]. The XRD patterns of all BG powders before and after thermal treatments are shown in Fig. 2C.

### 3.2. Dissolution study

The bone-bonding ability of BGs is usually qualitatively indicated by the formation of carbonated hydroxyapatite (HCA) layers on their surfaces upon immersion in simulated body fluid (SBF). Fig. 3 shows the XRD patterns of all BG powders after 7 days of immersion in SBF. A semi-crystalline phase with a prominent crystalline peak at 2 theta of 28° and 32° is observed, corresponding to the formation of a HCA layer [34,35].

Fig. 4 (A and B) represents the ion release profile for all investigated glasses, which was measured using ICP-OES. The displayed data shows only the released values at each time point. The amount of released copper ions was not detected under the measurement conditions, likely due to the fact that the concentration of copper ions released was lower than the detection limit of the instrument used. No significant difference in ion release was measured between the three glass compositions. The release of Na ions increases over the incubation time. While Si, Ca, and P ions' release stays nearly constant with incubation time. The amount of K ions increases in the solution. As a comparison, the ions released from glassy and fully crystalline F3 particles (size fraction of 500–600 μm) were also investigated (Fig. 4 C). A similar trend was measured for pure amorphous glasses. A slight difference in phosphorous ion release was noticed in the case of crystalline particles.

### 3.3. Sintered glasses

All glass compositions exhibited sufficient densification. The powder compacts of 13–93 BG showed a relative green body density 65 ±1 % and a compact density of 92 ±2 % after complete sintering. Compacts made from F3 BG show relative densification from 54 % to 88 %, and these made from F3–Cu composition densified from 52 % to 92 %. These relative green densities were calculated manually from the weight and geometry of the samples. Fig. 5a shows the surface of the sintered 13–93 powder compact before and after grinding with SiC paper of grade 1200 and 2000. Fig. 5b only shows the pellets of F3 and F3–Cu after final grinding with SiC disc grade 2000 observed with LSM. The measured roughness data for all surfaces are summarised in Table 3. All polished pellets revealed a high densification with only a few round pores. For F3 and F3–Cu samples, the pores are partially irregularly shaped. The surface of the sintered 13–93 pellet is already very smooth, and after grinding with SiC 1200, local spalling, chipping, and scratches are visible. Only flat scratches remain after the SiC 2000 grinding, and the measured roughness of peak to valley value, Sz, decreases to around a third. The average roughness Sa, also decreased to nearly a quarter of the previous value.

### 3.4. Cytocompatibility assessment

#### 3.4.1. Indirect study

Fig. 6 shows the cell viability (%) of aliquots of milled BG powders (D50 < 15 μm) after 1 and 3 days of incubation in cell culture medium. The dissolution products of all bioactive glasses strongly affected the cell viability. Initially, after 1 day, aliquots of F3–Cu showed toxicity toward MC3T3-E1 cells. However, the cell viability increased after 3 days of incubation. It can be anticipated that cells which remain alive after 1 day will potentially proliferate and duplicate. Overall, aliquots of 13–93 BG showed higher cell viability when compared with the positive control (Tissue culture plate) and other samples, suggesting a positive effect of the BG dissolution products on cell proliferation. On the other hand, the results indicated a decrease in viability for F3 and F3–Cu dissolution products. This could be due to the release of alkali content (Floride ions) or copper ions, which potentially suppress cell viability. Lin et al. [36] investigated the in vitro cytocompatibility of copper-doped 13–93 BG scaffolds using MC3T3-E1 cells. The proliferation and alkaline phosphatase activity results were found to be dose-dependent and were not affected by 0.4 and 0.8 wt% CuO in the glass, but they were significantly reduced by adding 2.0 wt% CuO. According to the measured composition in Table 1, F3–Cu glass contains ≈1.8 wt% CuO, e.g. a value potentially leading to cytotoxic effects, according to Lin et al.'s finding [36].

Fig. 7 presents the fluorescence microscopy images of MC3T3-E1 cells from indirect cell studies after 3 days of incubation. The fluorescence images confirm cell attachment, and the cells exhibit the characteristic morphology anticipated for biocompatible materials. The fluorescence microscopy results also agree with the percentage of cell viability results (Fig. 6). Similar behaviour of 13–93 BG has been reported in the literature when the BG was in contact with pre-osteoblast cells [25,37].

#### 3.4.2. Direct study

Surface roughness plays an important role in the attachment and proliferation of cells. The sintered/unpolished pellets and pellets polished with 1200 SiC paper show less cell viability. Cells were spread in the direction of scratches (data not shown here). Therefore, pellets polished with 2000 SiC paper were selected to compare the three different glasses, 13–93, F3 and F3–Cu. Fig. 8B represents the morphology and proliferation of cells on the surface of all pellets after polishing with 2000 SiC paper. Typical morphology of MC3T3-E1 cells

was observed, and SEM images show that cells are well spread after 5 days of seeding and are firmly attached to the surface of pellets. Cells have entirely covered the surface of F3 and F3–Cu samples are seen to be elongated, adopting a guided morphology. It is apparent that cell growth is guided by surface roughness, mainly the shallow scratches left behind from grinding. Fig. 8 A represent the cell viability (%) of polished pellets after 5 days of incubation in cell culture medium. The results were similar to indirect viability results. 13–93 BG samples showed highest viability compared to F3 and F3–Cu samples.

Overall, the cell viability and morphology confirm that the investigated BGs are biocompatible and support the proliferation and attachment of MC3T3-E1 cells. The indirect studies showed that dissolution products of all BGs strongly affected cell viability. In the direct approach, surface topography plays a vital role in cell proliferation, and cells were attached and guided along the direction of scratches. The results indicate that a synergistic effect between topography and ion dissolution products can be exploited to enhance the cell-BG surface interactions.

## 4. Conclusions

This study has investigated the dissolution and cytocompatibility of three different bioactive glasses. Regarding acellular scaffold's bioactivity, all powders revealed hydroxyapatite formation on their surfaces after seven days of immersion in simulated body fluid. Preliminary cell culture results showed dose-dependent cytocompatibility after exposure to BG ionic dissolution products using pre-osteoblast cells (MC3T3-E1). In the first 24 h, the dissolution products of F3–Cu BG led to toxicity. The composition and subsequent release kinetics of various ions from different BG types, such as 13–93, F3 and F3–Cu, affect cytocompatibility. No significant difference in ion release from amorphous powders was measured, as well as for glassy and fully crystallized F3 particles. The cell morphological results showed that surface topography affected cell proliferation, and cells were attached in a guided manner along the direction of scratches, which were left by the polishing procedure. Overall, the cell viability and morphology results confirm that the investigated BGs are biocompatible and support the proliferation and attachment of MC3T3-E1 cells.

## Declaration of competing interest

The authors declare that they have no known competing financial interests or personal relationships that could have appeared to influence the work reported in this paper.

## Acknowledgement

We gratefully acknowledge experimental support by our colleague M. Lindemann for ICP-OES analysis from Bundesanstalt für Materialforschung und -prüfung (BAM). Financial support by the Deutsche Forschungsgemeinschaft DFG (MU 963/18–1) and (BO 1191/29–1) is gratefully acknowledged.

## References

[1] S. Bose, D. Ke, H. Sahasrabudhe, A. Bandyopadhyay, Additive manufacturing of biomaterials, Prog. Mater. Sci. 93 (2018) 45–111.
[2] C. Garot, G. Bettega, C. Picart, Additive manufacturing of material scaffolds for bone regeneration: toward application in the clinics, Adv. Funct. Mater. 31 (2021).
[3] E. Pirhonen, H. Niiranen, T. Niemelä, M. Brink, P. Törmälä, Manufacturing, mechanical characterization, and in vitro performance of bioactive glass 13–93 fibers, J. Biomed. Mater. Res. Part B Appl. Biomater. An Off. J. Soc. Biomater. Japanese Soc. Biomater. Aust. Soc. Biomater, Korean Soc. Biomater. 77 (2006) 227–233.
[4] R. Gmeiner, U. Deisinger, J. Schönherr, B. Lechner, R. Detsch, A.R. Boccaccini, J. Stampfl, Additive manufacturing of bioactive glasses and silicate bioceramics, J. Ceram. Sci. Technol. 6 (2015) 75–86.
[5] L. Lefebvre, L. Gremillard, J. Chevalier, R. Zenati, D. Bernache-Assolant, Sintering behaviour of 45S5 bioactive glass, Acta Biomater. 4 (2008) 1894–1903.
[6] C. Blaeß, R. Müller, G. Poologasundarampillai, D.S. Brauer, Sintering and concomitant crystallization of bioactive glasses, Int. J. Appl. Glass Sci. 10 (2019) 449–462.
[7] I. Kinnunen, K. Aitasalo, M. Pöllönen, M. Varpula, Reconstruction of orbital floor fractures using bioactive glass, J. Cranio-Maxillofacial Surg. 28 (2000) 229–234.
[8] R.G. Hill, D.S. Brauer, Predicting the bioactivity of glasses using the network connectivity or split network models, J. Non-Cryst. Solids 357 (2011) 3884–3887.
[9] A.R. Boccaccini, Q. Chen, L. Lefebvre, L. Gremillard, J. Chevalier, Sintering, crystallisation and biodegradation behaviour of Bioglass®-derived glass–ceramics, Faraday Discuss 136 (2007) 27–44.
[10] O. Bretcanu, X. Chatzistavrou, K. Paraskevopoulos, R. Conradt, I. Thompson, A. R. Boccaccini, Sintering and crystallisation of 45S5 Bioglass® powder, J. Eur. Ceram. Soc. 29 (2009) 3299–3306.
[11] J. Massera, S. Fagerlund, L. Hupa, M. Hupa, Crystallization mechanism of the bioactive glasses, 45S5 and S53P4 613 (2012) 607–613.
[12] O. Guillon, S. Cao, J. Chang, L. Wondraczek, A.R. Boccaccini, Effect of uniaxial load on the sintering behaviour of 45S5 Bioglass® powder compacts, J. Eur. Ceram. Soc. 31 (2011) 999–1007.
[13] H. Elsayed, A. Zocca, E. Bernardo, C.M. Gomes, J. Günster, P. Colombo, Development of bioactive silicate-based glass-ceramics from preceramic polymer and fillers, J. Eur. Ceram. Soc. 35 (2015) 731–739.
[14] P. Tesavibul, R. Felzmann, S. Gruber, R. Liska, I. Thompson, A.R. Boccaccini, J. Stampfl, Processing of 45S5 Bioglass® by lithography-based additive manufacturing, Mater. Lett. 74 (2012) 81–84.
[15] M. Brink, The influence of alkali and alkaline earths on the working range for bioactive glasses, J. Biomed. Mater. Res. An Off. J. Soc. Biomater. Japanese Soc. Biomater. 36 (1997) 109–117.
[16] I. Elgayar, A.E. Aliev, A.R. Boccaccini, R.G. Hill, Structural analysis of bioactive glasses, J. Non-Cryst. Solids 351 (2005) 173–183.
[17] M. Brink, T. Turunen, R. Happonen, A. Yli-Urpo, Compositional dependence of bioactivity of glasses in the system Na2O-K2O-MgO-CaO-B2O3-P2O5-SiO2, J. Biomed. Mater. Res. An Off. J. Soc. Biomater. Japanese Soc. Biomater. 37 (1997) 114–121.
[18] K.C.R. Kolan, A. Thomas, M.C. Leu, G. Hilmas, In vitro assessment of laser sintered bioactive glass scaffolds with different pore geometries, Rapid Prototyp. J. (2015).
[19] K.C.R. Kolan, M.C. Leu, G.E. Hilmas, M. Velez, Effect of material, process parameters, and simulated body fluids on mechanical properties of 13-93 bioactive glass porous constructs made by selective laser sintering, J. Mech. Behav. Biomed. Mater. 13 (2012) 14–24.
[20] G. Luo, Y. Ma, X. Cui, L. Jiang, M. Wu, Y. Hu, Y. Luo, H. Pan, C. Ruan, 13-93 bioactive glass/alginate composite scaffolds 3D printed under mild conditions for bone regeneration, RSC Adv. 7 (2017) 11880–11889.
[21] R. Meszaros, R. Zhao, N. Travitzky, T. Fey, P. Greil, L. Wondraczek, Three-dimensional printing of a bioactive glass, Glas. Technol. J. Glas, Sci. Technol. Part A. 52 (2011) 111–116.
[22] W. Xiao, M.A. Zaeem, B.S. Bal, M.N. Rahaman, Creation of bioactive glass (13–93) scaffolds for structural bone repair using a combined finite element modeling and rapid prototyping approach, Mater. Sci. Eng. C 68 (2016) 651–662.
[23] Y. Cao, B. Yang, C. Gao, P. Feng, C. Shuai, Laser sintering of nano 13-93 glass scaffolds: microstructure, mechanical properties and bioactivity, Sci. Sinter. 47 (2015).
[24] A. Winkel, R. Meszaros, S. Reinsch, R. Müller, N. Travitzky, T. Fey, P. Greil, L. Wondraczek, Sintering of 3 D-printed glass/HA p composites, J. Am. Ceram. Soc. 95 (2012) 3387–3393.
[25] T.H. Qazi, S. Hafeez, J. Schmidt, G.N. Duda, A.R. Boccaccini, E. Lippens, Comparison of the effects of 45S5 and 1393 bioactive glass microparticles on hMSC behavior, J. Biomed. Mater. Res., Part A 105 (2017) 2772–2782.
[26] D. Groh, F. Döhler, D.S. Brauer, Bioactive glasses with improved processing. Part 1. Thermal properties, ion release and apatite formation, Acta Biomater. 10 (2014) 4465–4473.
[27] S. Schaefer, R. Detsch, F. Uhl, U. Deisinger, G. Ziegler, How degradation of calcium phosphate bone substitute materials is influenced by phase composition and porosity, Adv. Eng. Mater. 13 (2011) 342–350.
[28] M. Plewinski, K. Schickle, M. Lindner, A. Kirsten, M. Weber, H. Fischer, The effect of crystallization of bioactive bioglass 45S5 on apatite formation and degradation, Dent. Mater. 29 (2013) 1256–1264.
[29] N.C. Lindfors, J.T. Heikkilä, I. Koski, K. Mattila, A.J. Aho, Bioactive glass and autogenous bone as bone graft substitutes in benign bone tumors, J. Biomed. Mater. Res. Part B Appl. Biomater. 90 (2009) 131–136.
[30] C. Blaeß, R. Müller, G. Poologasundarampillai, D.S. Brauer, Sintering and concomitant crystallization of bioactive glasses, Int. J. Appl. Glass Sci. 10 (2019) 449–462.
[31] F. Döhler, D. Groh, S. Chiba, J. Bierlich, J. Kobelke, D.S. Brauer, Bioactive glasses with improved processing. Part 2. Viscosity and fibre drawing, J. Non-Cryst. Solids 432 (2016) 130–136.
[32] T. Kokubo, H. Takadama, How useful is SBF in predicting in vivo bone bioactivity? Biomaterials 27 (2006) 2907–2915.
[33] O. Bretcanu, X. Chatzistavrou, K. Paraskevopoulos, R. Conradt, I. Thompson, A. R. Boccaccini, Sintering and Crystallisation of 45S5 Bioglass ® Powder, vol. 29, 2009, pp. 3299–3306.
[34] K. Zheng, X. Dai, M. Lu, N. Huser, N. Taccardi, A.R. Boccaccini, Synthesis of copper-containing bioactive glass nanoparticles using a modified Stober method for biomedical applications, Colloids Surf. B Biointerfaces 150 (2017) 159–167.

[35] K. Zheng, X. Dai, M. Lu, N. Hüser, N. Taccardi, A.R. Boccaccini, Synthesis of copper-containing bioactive glass nanoparticles using a modified Stöber method for biomedical applications, Colloids Surf. B Biointerfaces 150 (2017) 159–167.
[36] Y. Lin, W. Xiao, B.S. Bal, M.N. Rahaman, Effect of copper-doped silicate 13–93 bioactive glass scaffolds on the response of MC3T3-E1 cells in vitro and on bone regeneration and angiogenesis in rat calvarial defects in vivo, Mater, Sci. Eng. C. 67 (2016) 440–452.
[37] Q. Fu, M.N. Rahaman, B.S. Bal, R.F. Brown, D.E. Day, Mechanical and in vitro performance of 13–93 bioactive glass scaffolds prepared by a polymer foam replication technique, Acta Biomater. 4 (2008) 1854–1864.